The local structure and ferromagnetism in Fe-implanted SrTiO3 single crystals

O. Lobacheva, M. Chavarha, Y. M. Yiu, T. K. Sham, and L. V. Goncharova

Citation: Journal of Applied Physics **116**, 013901 (2014); doi: 10.1063/1.4886875
View online: http://dx.doi.org/10.1063/1.4886875
View Table of Contents: http://scitation.aip.org/content/aip/journal/jap/116/1?ver=pdfcov
Published by the AIP Publishing

The local structure and ferromagnetism in Fe-implanted $SrTiO_3$ single crystals

O. Lobacheva,[1,a)] M. Chavarha,[1] Y. M. Yiu,[2] T. K. Sham,[1,2] and L. V. Goncharova[1,2]
[1]*Department of Physics and Astronomy, The University of Western Ontario, London ON N6A 5B7, Canada*
[2]*Department of Chemistry, The University of Western Ontario, London ON N6A 5B7, Canada*

(Received 29 April 2014; accepted 23 June 2014; published online 1 July 2014)

We report a connection between the local structure of low-level Fe impurities and vacancies as the cause of ferromagnetic behavior observed in strontium titanate single crystals (STO), which were implanted with Fe and Si ions at different doses then annealed in oxygen. The effects of Fe doping and post-implantation annealing of STO were studied by X-ray Absorption Near Edge Structure (XANES) spectroscopy and Superconducting Quantum Interference Device magnetometry. XANES spectra for Fe and Ti K- and L-edge reveal the changes in the local environment of Fe and Ti following the implantation and annealing steps. The annealing in oxygen atmosphere partially healed implantation damages and changed the oxidation state of the implanted iron from metallic Fe^0 to Fe^{2+}/Fe^{3+} oxide. The STO single crystals were weak ferromagnets prior to implantation. The maximum saturation moment was obtained after our highest implantation dose of 2×10^{16} Fe atom/cm^2, which could be correlated with the metallic Fe^0 phases in addition to the presence of O/Ti vacancies. After recrystallization annealing, the ferromagnetic response disappears. Iron oxide phases with Fe^{2+} and Fe^{3+} corresponding to this regime were identified and confirmed by calculations using Real Space Multiple Scattering program (FEFF9). © *2014 AIP Publishing LLC*.
[http://dx.doi.org/10.1063/1.4886875]

INTRODUCTION

Strontium titanate $SrTiO_3$ (STO) is an important technological material due to its high chemical and thermal stability, high dielectric constant and resistance to oxidation. Its numerous applications include standard substrates for epitaxial growth, electro-optical devices, gas sensors, photocatalysts, oxide cathodes, insulating layers in random access memory, ferroelectric thin film structures, high-T_C superconductors, and potential gate dielectric material.[1–5] Recently, relatively defect-free STO epitaxial oxides have been successfully grown on Si;[6,7] however, the ideal epitaxial $SrTiO_3$/Si structures are meta stable at best, and interfacial layer compositions often differ from theoretical prediction.[8] STO doped with transition metals is among several oxide materials that attract considerable attention as a suitable material for spintronic applications.[9–11] Despite some progress in this area, the origin of the observed ferromagnetism is still under debate. Though previous studies showed that ferromagnetism in these materials was largely due to iron contamination introduced during fabrication, defect-related ferromagnetism was also reported.[12,13] Magnetic properties of these systems can be explained by charge transfer between defect states and doping ions.[14] Defects form a narrow band with high density of states in the vicinity of the Fermi level, while transition metal ions with variable valence act as a charge reservoir to or from which electrons can be transferred to the defect bands. The challenge, here, is the uncontrollable nature of defects that are usually not in thermodynamic equilibrium, and their concentration and distribution can change irreversibly upon heating. Theoretical calculations conducted on STO super-cell structures show that oxygen vacancies have a tendency to form clusters.[15–17]

In this work, we explore the origin of magnetism produced by implantation of Fe (magnetic) and Si (non-magnetic) ions into a STO substrate followed by annealing. STO single crystals were doped with Fe by ion beam implantation to introduce Fe doping in a controlled way. Several implantation doses were chosen to be consistent with the typical levels of Fe contaminations for commercial, un-polished single crystal STO samples, as measured by particle-induced X-ray emission spectroscopy.[12] Implantation and defect profiles were predicted using the Stopping and Range of Ions in Matter (SRIM),[18] a Monte Carlo simulation code. Local chemical phases of the resultant Fe impurities were identified by X-ray Absorption Near Edge Structure (XANES). Superconducting Quantum Interference Device (SQUID) analysis of STO samples of interest was conducted to find the correlation between observed magnetic behavior, Fe phases, defect concentration and order.

EXPERIMENTAL DETAILS

$SrTiO_3$ (001) single crystal substrates ($5 \times 5 \times 0.5$ mm^3 with both face polished) were purchased from MTI Crystals, Inc. (USA). Implantation with Fe and Si ions was performed at the Tandetron facility, the University of Western Ontario, Canada at room temperature with 30 keV Fe^+ ions, at an angle of incidence of 7° off normal to avoid channeling, $p = 5 \times 10^{-8}$ Torr. The STO substrates were implanted with

a)Author to whom correspondence should be addressed. Electronic mail: olobache@uwo.ca

iron at doses of 2×10^{14}, 8×10^{14}, and 2×10^{16} Fe ion/cm^2 and henceforth denoted as STO-214, STO-814, and STO-216, respectively. These samples were annealed for 2 h at 350 °C in O_2 atmosphere to prevent additional oxygen vacancy (V_O) formation. These samples were denoted as STO-214–350, STO-814–350, and STO-216–350, respectively. According to SRIM, 30 keV Fe is distributed in the near-surface region of ~50 nm thick, with the maximum of the implanted irons distributed at a depth of ~20 nm. Defects, mainly oxygen vacancies, produced during implantation are concentrated at the same depth, with the maximum closer to the surface. Annealing induces recrystallization and redistribution of defects formed due to irradiation damage. The Si-implanted STO sample, STO-Si, was fabricated with 90 keV Si^+ ions, 7° off normal, at a dose of 2×10^{16} Si ion/cm^2. The dose was chosen so that the spatial distribution of oxygen vacancies was about the same as in the sample STO-216.

XANES was used to identify chemical phases of Fe in STO. XANES is an element and oxidation state specific method, tracking the local structure and bonding of the absorbing atom.[19] Experiments were performed at the Canadian Light Source (CLS) (Saskatoon, Canada) and the Advanced Photon Source (APS) at Argonne National Laboratory (Argonne, IL, USA). At CLS, XANES measurements of the Ti and Fe L-edges were performed at the high resolution Spherical Grating Monochromator (SGM) beamline, which uses a 45 magnet planar undulator and three gratings covering an X-ray photon energy range from 250 to 2000 eV. It provides resolution greater than 5000 E/ΔE at energy below 1500 eV and better than 10 000 E/ΔE at the N K-edge. The photon energy was calibrated at C K-edge at 284.2 eV. At APS, Ti K-edge and Fe K-edge XANES measurements were made at the PNC/XSD beamline (20-BM), which uses Si double-crystal monochromator to cover a photon energy range of ~5–25 keV and offers resolution greater than 7000 E/ΔE. The double-crystal monochromator photon energy was calibrated at the Fe K-edge threshold of an iron foil at 7110.6 eV. The absorption spectra were collected in the total fluorescence yield (TFY) and total electron yield (TEY) at the CLS. For the L-edge measurements, TEY is more surface sensitive than TFY due to the short escape depth of electrons in matter. At APS, XANES spectra were collected in TFY mode using s Si drift fluorescence detector.

Measurements of the field-dependent magnetization were done at 5 K and 300 K using a Quantum Design SQUID magnetometer on the same samples at the Institute of Materials Research (IMR) of the Dalhousie University. Temperature dependence magnetization measurements were done at 500 Oe and at zero fields, for the selected samples with obvious hysteresis loops at room temperature.

RESULTS AND DISCUSSION

Figure 1(a) shows the Fe K-edge XANES of the implanted STO-216 and annealed STO-216–350. For comparison, the spectra of iron foil and iron oxide Fe_2O_3 are also given. The STO features (see Figure 1(a)) are not as sharp as those of the iron foil and iron oxide. The broadening and

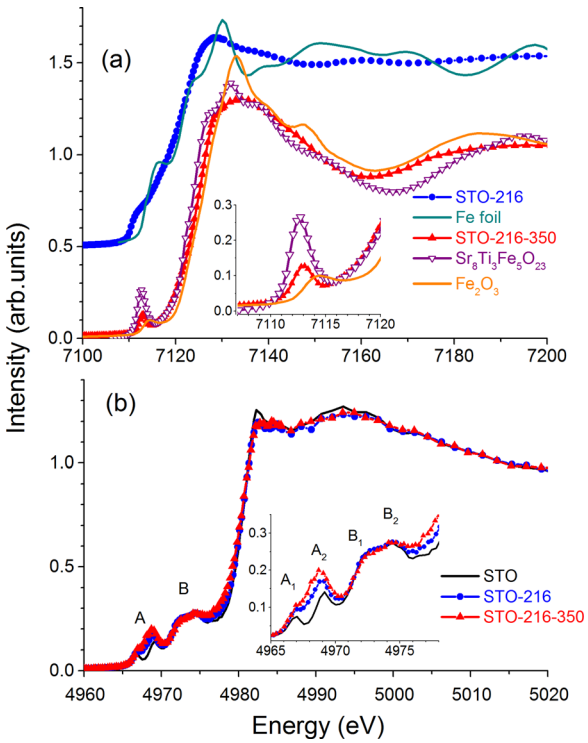

FIG. 1. (a) Fe K-edge and (b) Ti K-edge XANES spectra of STO samples: un-implanted STO crystal (solid black line), implanted with Fe STO-216 (solid circles), and implanted and annealed STO-216-350 (triangles). Experimental iron foil, iron oxide Fe_2O_3, and calculated $Sr_8Ti_3Fe_5O_{23}$ cluster (open triangles) spectra are also shown for comparison. Fe K-edge spectra are arbitrarily shifted along the vertical axis for clarity.

disappearance of the oscillations above the absorption edge suggest that implanted iron does not have long-range order. There is a distinct difference between the Fe K-edge spectra of STO-216 and STO-216–350. The shoulder at ~7112 eV in the pre-edge region indicates that in the as-implanted STO-216 sample, iron is in the Fe^0 oxidation state and is metallic. The Fe K-edge spectrum of the STO-216–350 has a sharp pre-edge peak at ~7113 eV, demonstrating that iron becomes Fe^{3+} after annealing in oxygen atmosphere. In *3d* metals, the pre-edge feature in the K-edge range is attributed to the *s-d* quadrupole transition due to *d-p* mixing. The pre-edge peak can provide information about oxidation state and the local coordination geometry of the metal atom (e.g., tetrahedral versus octahedral).[20,21] A comparison with Fe_2O_3 standard spectrum (Fig. 1(a), inset) shows that the pre-edge feature of STO-216–350 is more intense and moves to a lower energy, indicating that the Fe sites of STO-216–350 increasingly deviate from the centrosymmetric O_h geometry.[20,22]

The iron oxidation state before and after annealing can also be confirmed by the Fe L-edge XANES (Figure 2(a)). The position and shape of the resonances are sensitive to the local electronic structure, symmetry, and the oxidation state. The $L_{2,3}$ edges of 3*d* metals are dominated by very intense "white line" features due to *p-d* dipole transitions into the unoccupied *d* states. This transition is governed by a combined effect of the dominant crystal field splitting, band formation, spin orbit coupling, and final state exchange interaction.[23,24] Crystal field splitting of the *d* states can be

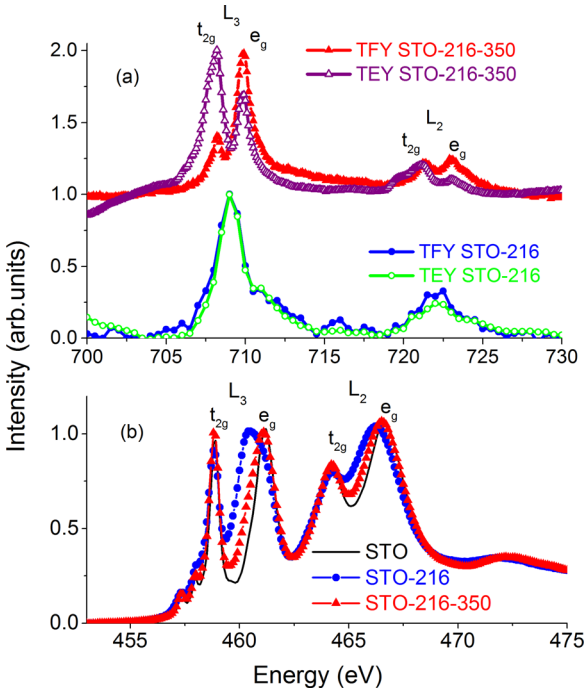

FIG. 2. (a) Fe L-edge and (b) Ti L-edge XANES spectra of STO samples: un-implanted STO crystal (solid black line), implanted with Fe STO-216 (solid circles), and implanted and annealed STO-216-350 (triangles). Spectra are shown in TFY (solid symbols) and TEY (open symbols). Fe L-edge spectra are arbitrarily shifted along the vertical axis for clarity.

observed as a splitting of the "white line" feature related to the t_{2g} and e_g final states in the octahedral field as is the case in STO. At the Fe L-edge, XANES were collected in the TFY and TEY. There are two single L_2 and L_3 peaks in the XANES for STO-216. Note that both TFY and TEY absorption peaks are identical but weak because the iron concentration in our samples is low and therefore there is no saturation effect in TFY. No iron peaks were detected in STO samples prior to implantation. For STO-814 sample, the L_2 and L_3 peaks were very weak and they were below the detection level for the low implantation dose (STO-214).

The lack of splitting of the "white line" feature of Fe $L_{3,2}$ absorption peaks of the STO-216 sample suggests that iron is in the metallic state Fe^0 in the as-implanted strontium titanate.[25] After annealing in oxygen atmosphere at 350 °C, the Fe $L_{3,2}$ absorption peaks of the STO-216–350 sample change into doublets, characteristic of Fe^{2+}/Fe^{3+} states. The intensity ratios of the doublets are different in TFY and TEY spectra. The intensity distributions of these doublets show that the first near edge peak of TEY is higher than that of TFY spectra. This feature is characteristic of Fe^{2+} and indicates that the iron oxidation state in the annealed sample of STO-216–350 corresponds to dominantly Fe^{2+} on TEY spectrum and Fe^{3+} on TFY spectrum.[26] Since TEY is more surface sensitive compared to the TFY, this corresponds to higher oxygen deficiency near the surface area of STO crystal compared to its bulk.

Ti K-edge XANES of the Fe-doped STO samples exhibit a pattern typical for the STO cubic perovskite structure (Figure 1(b)). The influence of the iron implantation and the post-implantation annealing is mostly noticeable in the pre-edge area (Figure 1(b), inset). Iron implantation and subsequent annealing lead to an increase in the intensity of the $A_{1,2}$ features compared to the un-implanted STO. This observed growth of the A pre-edge peaks intensity resulting from Fe doping is consistent with the findings of Ghaffari *et al.*[27] and Vracar *et al.*[28] who investigated $SrTi_{1-x}Fe_xO_{3-\delta}$ powders ($0 \leq x \leq 1$).

Ti $L_{2,3}$-edge XANES of STO samples are shown in Figure 2(b). The Ti $L_{3,2}$-edge spectra are dominated by dipole transitions between Ti $2p$ and Ti $3d$ levels. As was mention above L-edge spectra are sensitive to the local symmetry. Ti $L_{2,3}$-edge spectra clearly reflect the influence of ion implantation. There is a noticeable broadening and shift of the e_g peaks in the spectrum of the as-implanted STO-216 sample suggesting local distortion. During ion irradiation, a large amount of defects, mainly oxygen vacancies, was produced in the STO crystal.[18] To compensate for this, Ti ions move away from the oxygen vacancies and increase the effective Ti-O distance and therefore shift e_g peaks to lower energies, this is accompanied by a distortion of the O_h symmetry locally as is the case in the Ti $L_{3,2}$ edge of TiO_2 rutile and anatase.[29] In the spectrum of the annealed STO-216–350 sample, the peak narrows and the position of e_g peaks moves back toward that of the un-implanted STO crystal. This indicates that oxygen anneal removes most of the oxygen vacancies but not completely.

Overall, the XANES results strongly suggest that iron in STO crystal after implantation is in a metallic state, most likely forming small clusters. Annealing in oxygen causes iron to oxidize and incorporate partially into the crystal structure of strontium titanate substituting Ti ions, and it probably forms small clusters of either γ-Fe_2O_3 or $SrTi_{1-x}Fe_xO_{3-\delta}$. Because of the difference in oxidation state of Ti^{4+} and $Fe^{3+/2+}$ ions, presence of oxygen vacancies is required to maintain the electron neutrality of the STO crystal. We have performed the Real Space Multiple Scattering calculation using FEFF9 (Refs. 30 and 31) on a $2 \times 2 \times 2$ supercell (40 atoms) of STO structure. The $Sr_8Fe_8O_{23}$ supercell (8 STO lattice units with one oxygen vacancy) produces a good fit for the experiment spectrum of STO-216–350. The best approximation to our experimental data is $Sr_8Ti_3Fe_5O_{23}$ cluster with one oxygen vacancy and several Ti ions replaced by Fe. The FEFF9 result is shown in Figure 1(a). Previously, Lenser *et al.*[32] demonstrated that the degree of association of Fe and oxygen vacancies (Fe^{3+}–V_O) has a tendency to decrease with increasing doping level. Since doping level is small in our samples compared to the solid state solutions studied by others, we expect a strong connection between Fe and oxygen vacancy sites. The difference in the Fe oxidation state (Fe^{2+} and Fe^{3+}) distributions from Fe L-edge XANES collected in TEY and TFY modes indicates that oxygen vacancies are most likely located near the surface layers and on the iron oxide clusters boundaries.

Recently, Fe-implanted $SrTiO_3$ structures were investigated using depth-selective conversion electron Mössbauer spectroscopy and surface magneto-optical Kerr effect (SMOKE) by Dulov *et al.*[10] They identified that the origin of magnetism is α-Fe metallic nanoparticles with estimated average particle size of 5 nm for all implantation doses

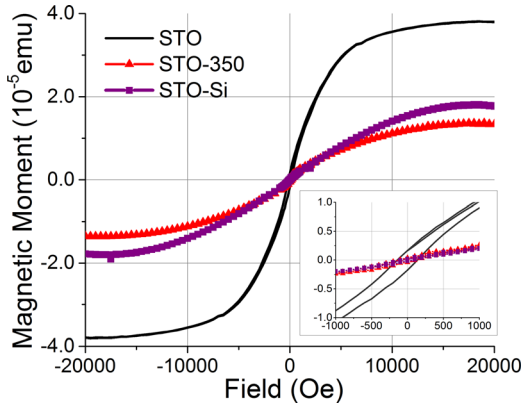

FIG. 3. Magnetic moment vs. applied field curves measured at 5 K for STO samples: un-implanted STO crystal (solid line), un-implanted and annealed in oxygen at 450 °C sample STO-350 (triangles), and Si implanted sample STO-Si (squares). Insets: enlarged image demonstrates the absence of the ferromagnetic hysteresis for STO-Si.

($7.5 \times 10^{16} - 1.5 \times 10^{17}$ Fe ion/cm^2). Additionally, they postulated substitution of the host Ti^{4+} ions with Fe^{2+} and Fe^{3+} in the sample with an implantation dose of 7.5×10^{16} Fe ion/cm^2), which is consistent with our results except that we observe Fe^{2+} and Fe^{3+} phases only after high temperature anneal.

Magnetic moment (M) vs. field (H) curves of all STO samples show both linear diamagnetic and nonlinear ferromagnetic behavior due to the intrinsic diamagnetic nature of strontium titanate since only a near-surface layer of STO crystal substrate is affected by implantation. The linear diamagnetic contribution was subtracted from M(H) curves by making linear fits in the higher field regions ($-5000 \leq H \leq -2000$ and $2000 \leq H \leq 5000$ G) to quantify saturation moments for implanted and un-implanted samples (Figures 3 and 4).

Notably, un-implanted two-side polished STO crystal has a weak magnetic moment. Previous studies showed that surface contaminations are often responsible for the magnetism of strontium titanate crystals, in the presence of ferromagnetic impurities. The studies showed that when magnetic impurities were deleted by the surface polishing, the initial magnetic moment of several oxide substrates decreased significantly.[8,12] In an alternative studies,[33] the effects of oxygen vacancies on the ferromagnetism in rutile TiO_2 have also been demonstrated based on first-principles local density approximation (LDA + U) calculations. Their results show that the magnetic moment depends on the oxygen vacancies concentration x, and predicted the ferromagnetism in rutile TiO_{2-x} with $x > 0.0417$. Oxygen vacancies not only modulate the valence of neighboring transition metal elements but also cause a change of the band structure of the host oxides. Therefore, one can achieve ferromagnetism by increasing vacancy concentrations above certain threshold, while still keeping ordering within the crystalline lattice of the host material. And experimentally, oxygen anneal typically decreased magnetic moment in contrast to vacuum anneal.[12]

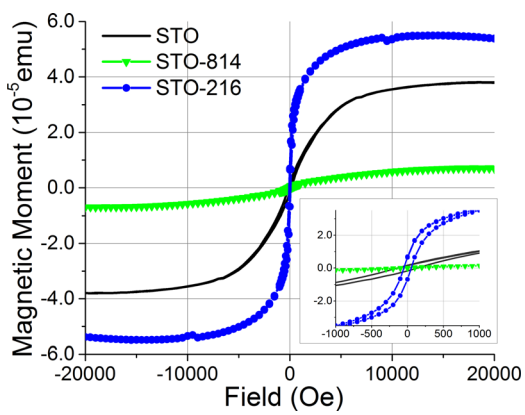

FIG. 4. Magnetic moment vs. applied field curves measured at 5 K for STO samples: un-implanted STO crystal (solid line), as-implanted STO-814 (triangles), and as-implanted STO-216 (solid circles). Insets: enlarged image demonstrates ferromagnetic hysteresis for STO-216.

In our as-purchased two-side polished STO samples, the level of magnetic impurities was below the detection level of particle-induced X-ray emission, X-ray photoelectron spectroscopy, and XANES. So we argue that the initial magnetic moments of STO crystal used in this study must be due to the ordered defects such as oxygen vacancies. We can decrease the number of oxygen vacancies by heating in oxygen, or we can destroy ordering in host oxide lattice by ion bombardment. STO crystals annealed in oxygen atmosphere at 350 °C have magnetic moment lower roughly by a factor of three, compared to untreated STO crystal (Figure 3).

To further explore the role of oxygen vacancies in the magnetic properties, STO substrate was implanted with nonmagnetic silicon ions. Though the implanted layer in STO-Si sample was thicker than that in the Fe ion implanted samples, the dose of 2×10^{16} Si ion/cm^2 produced comparable level of damage ($\sim 1.6 \times 10^{19}$ V_o/cm^2) but with nonmagnetic ions. These vacancies are abundant, however, they are not well ordered, and do not contribute to the magnetic moment. The M(H) curve for STO-Si sample after subtraction of the diamagnetic contribution is also presented in Figure 3. The Si implantation leads to reduction of the magnetic moment by approximately factor of two compared to the sample before implantation. We can speculate that if the second side of the sample was implanted with Si, we would bring the magnetic moment to zero. Additionally, Si-implanted sample exhibited no ferromagnetic hysteresis (Figure 3, inset), and the saturation of M(H) of STO-Si sample is reached at high values of magnetic field of 15 kOe, suggesting soft-ferromagnetic behavior.

Implantation of the high dose of iron of 2×10^{16} ion/cm^2 yields a magnetic moment with a ferromagnetic hysteresis loop (Figure 4, inset). Remarkably, STO-814 sample with medium implantation dose of Fe has a lower magnetic moment compared to un-implanted STO crystal (Figure 4). Ion implantation introduces disordering to the crystal structure. The disordering diminishes the initial magnetic moment of the un-implanted strontium titanate crystals, and the dose of Fe doping in STO-814 sample has been too low to produce nucleation of any Fe phases, which could increase magnetic moment.

Post-implantation annealing in oxygen of sample STO-216–350 leads to decrease in magnetic moment to zero (not shown here). Post-implantation annealing in oxygen

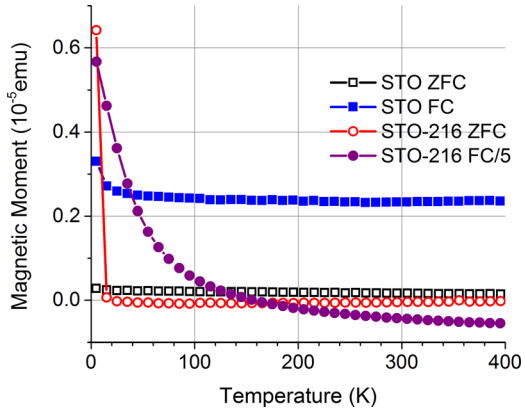

FIG. 5. Temperature dependent magnetization M(T) curves of un-implanted STO (squares) and as-implanted STO-216 (circles) samples (ZFC and FC, 500 Oe and are shown in open and solid symbols, respectively). M(T) curve of sample STO-216 acquired in field cooling implementation is divided by factor of 5.

contributes to two different effects. First, it partially heals oxygen vacancies produced during ion implantation. Second, it reduces ferromagnetic domains due to Fe^0. We infer from our XANES results that after anneal in oxygen iron incorporates partially into the crystal structure of STO substituting Ti ions. The process destroys the ferromagnetic order, and the implanted and, then, annealed STO-216–350 sample becomes purely diamagnetic.

Figure 5 shows magnetization curves of zero field cooled (ZFC) and field cooled samples under an applied field of 500 Oe (FC). Temperature dependent magnetic moment M(T) of all tested samples shows monotonous decrease with temperature. No noticeable transitions were found on M(T) curves in the 5–400 K range. The presented M(T) curves show that magnetic behavior of STO samples is mostly diamagnetic or paramagnetic.

CONCLUSIONS

In conclusion, it has been demonstrated that iron impurities in oxidation state Fe^0 can be an unambiguous ferromagnetic contribution to the magnetization for single crystal $SrTiO_3$ samples. Upon annealing, iron is oxidized to Fe^{3+} and Fe^{2+} in the near-surface layer, and oxygen-annealed samples become purely diamagnetic. Annealing in oxygen, thus, removes oxygen vacancies and destroys the original magnetic ordering, as well as it reduces domain size due to Fe^0. It is also possible to achieve soft ferromagnetic response by introducing a higher number of O/Ti vacancies, as we demonstrated that it can be done by Si ion implantation.

ACKNOWLEDGMENTS

This research was supported by the National Science and Engineering Research Council of Canada, the Canadian Foundation for Innovation, Canada Research Chairs (TKS), and the Ontario Ministry of Innovation. We would like to thank Jack Hendricks (Tandetron facility at University of Western Ontario) and Victoria Karner for their help with fabrication of the samples, Robert Gordon (Advanced Photon Source of Argonne National Laboratory and Canadian Light Source) and also Samer Kahwaji (MBE Lab of Dalhousie University) for his assistance with SQUID.

[1]Y. H. Jang, C. H. Kim, S. J. Seo, and J. H. Cho, Thin Solid Films **548**, 52 (2013).
[2]C. L. Chow, W. C. Ang, M. S. Tse, and O. K. Tan, Thin Solid Films **542**, 393 (2013).
[3]H. Liu, H. Dong, X. Meng, and F. Wu, Chem. Phys. Lett. **555**, 141 (2013).
[4]Ariando, X. Wang, G. Baskaran, Z. Q. Liu, J. Huijben, J. B. Yi, A. Annad, A. Roy Barman, A. Rusydi, S. Dhar, Y. P. Feng, J. Ding, H. Hilgenkamp, and T. Venkatesan, Nat. Commun. **2**, 188 (2011).
[5]J. H. Haeni, P. Irvin, W. Chang, R. Uecker, P. Reiche, Y. L. Li, S. Choudhury, W. Tian, M. E. Hawley, B. Craigo, A. K. Tagantsev, X. Q. Pan, S. K. Streiffer, L. Q. Chen, S. W. Kirchoefer, J. Levy, and D. G. Schlom, Nature **430**(7001), 758 (2004).
[6]J. Q. He, J. Appl. Phys. **97**, 104921 (2005).
[7]K. Eisenbeiser, J. M. Finder, Z. Yu, J. Ramdani, J. A. Curless, J. A. Hallmark, R. Droopad, W. J. Ooms, L. Salem, S. Bradshaw, and C. D. Overgaard, Appl. Phys. Lett. **76**, 1324 (2000).
[8]L. V. Goncharova, D. G. Starodub, E. Garfunkel, T. Gustafsson, V. Vaithyanathan, J. Lettieri, and D. G. Schlom, J. Appl. Phys. **100**, 014912 (2006).
[9]S. Kazan, A. G. Sale, J. I. Gatiiatova, V. F. Valeev, R. I. Khaibullin, and F. A. Mikailzade, Solid State Commun. **150**, 219 (2010).
[10]E. N. Dulov, N. G. Ivoilov, O. A. Strebkov, L. R. Tagirov, V. I. Nuzhdin, R. I. Khaibullin, S. Kazan, and F. A. Mikailzade, Mater. Res. Bull. **46**, 2304 (2011).
[11]Sendilkumar, P. D. Babu, M. M. Raja, V. R. Reddy, A. Gupta, and S. Srinath, J. Am. Ceram. Soc. **96**(9), 2973 (2013).
[12]D. A. Crandles, B. DesRoches, and F. S. Razavi, J. Appl. Phys. **108**, 053908 (2010).
[13]S. M. M. Yee, D. A. Crandles, and L. V. Goncharova, J. Appl. Phys. **110**, 033906 (2011).
[14]J. M. D. Coey, P. Stamenov, R. D. Gunning, M. Venkatesan, and K. Paul, New J. Phys. **12**, 053025 (2010).
[15]F. Cordero, Mater. Sci. Eng., A **521–522**, 77 (2009).
[16]M. Djermouni, A. Zaoui, S. Kacimi, and B. Bouhafs, Comput. Mater. Sci. **49**, 904 (2010).
[17]J. Robertson, J. Appl. Phys. **93**(2), 1054–1059 (2003).
[18]J. Ziegler, J. Biersack, and U. Littmark, *The Stopping and Ion Range of Ions in Matter* (Pergamon, New York, 1985).
[19]S. C. Ray, J. W. Chiou, and W. F. Pong, Crit. Rev. Solid State **31**, 91 (2006).
[20]T. E. Westre, P. Kennepohl, J. G. DeWitt, B. Hedman, K. O. Hodgson, and E. I. Solomon, J. Am. Chem. Soc. **119**, 6297 (1997).
[21]F. M. F. de Groot, J. Phys.: Conf. Ser. **190**, 012004 (2009).
[22]L. X. Chen, T. Liu, M. C. Thurnauer, R. Csencsits, and T. Rajh, J. Phys. Chem. B **106**, 8539 (2002).
[23]F. de Groot and A. Kotani, *Core Level Spectroscopy of Solids* (CRC Press, Boca Raton, 2008).
[24]T.-K. Sham, J. Chem. Phys. **83**, 3222 (1985).
[25]J. Leveneur, G. I. N. Waterhouse, J. Kennedy, J. B. Metson, and D. R. G. Mitchel, J. Phys. Chem. C **115**, 20978 (2011).
[26]S. Yang, D. Wang, G. Liang, Y. M. Yiu, J. Wang, L. Liu, X. Sun, and T.-K. Sham, Energy Environ. Sci. **5**, 7007 (2012).
[27]M. Ghaffari, T. Liu, H. Huang, O. K. Tan, and M. Shannon, Mater. Chem. Phys. **136**, 347 (2012).
[28]M. Vracar, A. Kuzmin, R. Merkle, J. Purans, E. A. Kotomin, J. Maier, and O. Mathon, Phys. Rev. B **76**, 174107 (2007).
[29]G. Zhu, G. Radtke, and G. A. Botton, Nature **490**, 384 (2012).
[30]J. J. Rehr, J. J. Kas, M. P. Prange, A. P. Sorini, Y. Takimoto, and F. Vila, C. R. Phys. **10**, 548–559 (2009).
[31]J. J. Rehr, J. J. Kas, F. D. Vila, M. P. Prange, and K. Jorissen, Phys. Chem. Chem. Phys. **12**, 5503–5513 (2010).
[32]C. Lenser, A. Kalinko, A. Kuzmin, D. Berzins, J. Purans, K. Szot, R. Waser, and R. Dittmann, Phys. Chem. Chem. Phys. **13**, 20779 (2011).
[33]G. Han, S. Hu, S. Yan, and L. Mei, Phys. Status Solidi RRL **3**(5), 148 (2009).